Mass Spectrometry Imaging in Nanomedicine

Mass spectrometry imaging in nanomedicine: unraveling the potential of MSI for detection of nanoparticles in neuroscience

Florian P.Y. Barré, Ron M. A. Heeren, Nina Ogrinc Potočnik

The Maastricht MultiModal Molecular Imaging Institute, M4I, Department of Imaging Mass Spectrometry, Maastricht University, Maastricht, The Netherlands

ABSTRACT

Mass spectrometry imaging (MSI) can uniquely detect thousands of compounds allowing both their identification and localization within biological tissue samples. MSI is an interdisciplinary science that crosses the borders of physics, chemistry and biology, and enables local molecular analysis at a broad range of length scales: From the subcellular level to whole body tissue sections. The spatial resolution of some mass spectrometers now allows nano-scale research, crucial for studies in nanomedicine. Recent developments in MSI have enabled the optimization and localization of drug delivery with nanoparticles within the body and in specific organs such as kidney, liver and brain. Combining MSI with nanomedicine has vast potential, specifically in the treatment of neurological disorders, where effective drug delivery has been hampered by the blood-brain barrier. This review provides an introduction to MSI and its different technologies, with the application of MSI to nanomedicine and the different possibilities that MSI offers to study molecular signals in the brain. Finally, we provide an outlook for the future and exciting potential of MSI in nanoparticle-related research.

KEYWORDS

mass spectrometry imaging; nanomedicine; brain; nanoparticles

INTRODUCTION

As the control center of the body, the brain regulates other organs and systems as well as gives rise to movement, thoughts, feelings, and memory. Concomitant with an increase in life expectancy, the brain has been subjected to a prolonged aging process and an increased risk for the development of neurodegenerative disorders such as Alzheimer's, Parkinson's and dementia. To date, there are no effective therapies for such diseases, especially due to the restricted passing of any potential treatment across the blood-brain barrier (BBB). The BBB, a semipermeable membrane formed by endothelial tight junctions, separates the blood vessels and the central nervous system (CNS). The BBB protects the brain by restricting passage of pathogens, toxins or hormones circulating in the blood. Unfortunately, this filter is too efficient and prohibits many active therapeutic molecules to reach the brain, complicating the treatment of many neurological diseases. Drug transit across the BBB is essential to treat some diseases such as cancer, Parkinson´s disease, Alzheimer´s disease and other neurological disorders. In recent years,

nanoparticles have emerged as the method with greatest potential for effective drug delivery due to their ability to maintain drug levels in the therapeutic range as well as to increase the half-life, solubility, stability and permeability of drugs across the BBB.[1] Thus, the detection and monitoring of nanoparticles as drug carriers are critical in drug discovery and development.

Mass spectrometry imaging (MSI) has demonstrated vast potential in clinical research and drug discovery, including its early application in the detection of nanoparticles. Mass spectrometry (MS) is a unique interdisciplinary technique combining physics, chemistry and biology to analyze the molecular composition of any sample. This technique allows us to understand biological processes from a sub- to multicellular level and from cells to whole biological systems. Initially, MS was predominantly used within the field of physics. A mass spectrometer measures the mass-to-charge ratios (*m/z*) of ions and can determine the molecule's mass if the charge is known. A mass spectrometer consists of three different parts: an ion source, which ionizes the analytes; mass analyzers, which separate the analytes based on their molecular weight and a detector that registers the presence of different analytes. With the development of soft ionization techniques in the 1980's, such as matrix-assisted laser desorption/ionization (MALDI)[2, 3] and electrospray ionization (ESI),[4] MS became more suitable for biological studies. Over the last three decades, MS has become an important analytical technique in biological and medical applications.

Based in MS, mass spectrometry imaging (MSI) developed as a relatively new technique to visualize and study the spatial distribution of biomolecules such as proteins, peptides, lipids, drugs and metabolites in biological tissue sections. Label-free imaging with mass spectrometry uses an intrinsic molecular parameter, the molecular mass, to visualize the distribution of a wide variety of biomolecules from sample surfaces. This is achieved by manipulating the ions in electric/magnetic fields or by measuring their time-of-flight (TOF). To use a mass spectrometer as an imaging instrument, the spectrometer needs to be equipped with a desorption and ionization source that can generate local information, an automated sample or beam manipulation system, automatic data acquisition and registration system and visualization software. The detected signal is proportional to the amount of the compound present in the sample. Each mass spectrum reflects the local molecular composition at a given pair of *x* and *y* coordinates. All locally acquired mass spectra from the tissue constitute an image dataset analogous to pixels in a digital photograph. Images show the distribution of the selected compound within the tissue section

according to the intensity distribution of a specific *m/z* value that is extracted from all the collected spectra. The relative abundance of that ion in each pixel can be visualized by a color intensity scale in a two-dimensional (2D) map. Images are generated by extracting data for the corresponding *m/z* ranges from the spatially acquired MS data files.

MSI provides *ex-vivo* molecular information that complements *in-vivo* and *in-vitro* imaging techniques, used for NP detection, such as magnetic resonance imaging (MRI),[5] positron emission tomography (PET),[6] autoradiography[7] or fluorescence imaging[8, 9] MSI does not require labelled molecules and can reach high spatial resolution (as low as 1 µm), two important advantages over other techniques. Furthermore, in a single experiment, thousands of molecules (targeted or untargeted) can be detected at the same time. Thus, MSI is suitable to study biodistributions in both large samples (rat or mouse whole-body tissue sections) and small tissue organs, such as the brain,[10] the kidney[11] or the eyes[12] with a relatively high spatial resolution. Subsequent developments that allowed instrument control as well as improved data acquisition and processing enabled imaging of endogenous compound distributions within thin tissue sections (**Figure 1**).

In the last decade, due to rapid instrumentation and sample preparation advances, the MSI approach expanded its range of applications in the pharmaceutical,[13] biomedical[14] and clinical fields.[15, 16] MSI is used in cancer research,[17, 18] ophthalmology,[12] degenerative diseases such as osteoarthritis[19] and neurology[20] but it is not limited to specific therapeutic areas. MSI instrumentation, methods and protocols have been developed to study the spatial distribution of endogenous compounds (such as lipids, peptides, and proteins) as well as exogenous compounds (such as polymers or pharmaceutical compounds) on complex surfaces. The imaging of pharmaceuticals and their metabolites is an essential source of information in drug discovery and development.[13] Here, we review different MSI innovations and how they are deployed in combination with newly developed nanoparticles based drug delivery systems in tissues and brain cells. MSI can follow and quantify the uptake of these nanoparticle carriers, the released drugs and their metabolites.

STATE OF THE ART IN MSI

Several reviews[21-23] have extensively covered various aspects of MSI technology and application. Below, we focus on three ionization techniques with the greatest potential to be used in nanomedicine: SIMS, MALDI and DESI (**Figure 2**).

Secondary ion mass spectrometry (SIMS) is the oldest MSI technique.[24, 25] Traditionally, SIMS has been applied in the domain of surface and solid-state physics. In SIMS, the sample surface is bombarded with primary ion particles, generating secondary ions that are analyzed. The primary ions, usually elemental ions generated from a liquid metal ion gun (LMIG), lose their energy (typically in 10–30 keV range) in electronic and nuclear collisions inside the target material.[26] Part of the energy is then transferred to other atoms and molecules, causing the secondary ions to be released from the sample surface. The particles are sputtered within 5–10 nm from the primary ion indent at high spatial resolution (as low as 50 nm). In the low-current static SIMS measurement, only one ion hits the local environment. Only a small fraction of atoms and molecules are ionized in the sputtering process, typically less than 1% of the total sputtered material, and form the basis of SIMS analysis.[27]

Over the several last years and with enhanced modifications, SIMS has been deployed in biomedical applications,[28] imaging cells[29] and tissue sections.[30] With different sample surface modifications, SIMS can analyze abundant lipids and small peptides.[31, 32] For matrix-enhanced (ME)-SIMS, the uppermost layer of the surface is covered with a matrix (ME-SIMS)[33, 34] in metal assisted (MetA)-SIMS, the top layer is sputter-coated with a thin layer of metal.[35-37] In both cases, the sputtering efficiency and the secondary molecular ion yield increases. Another advancement in SIMS technology was the replacement of the traditional LMIG sources by cluster ion sources (Au_n^+, Bi_n^+, SF_5^+,C_{60}^+, ...), which increased signal intensity, quality of the image and provided novel depth profiling capabilities.[38-41]

Recently, the energy range of primary ions used in SIMS has been moved from keV into the MeV domain, which has completely different desorption mechanisms. In contrast to low energy ions in the keV region, the MeV ion beams have the ability to desorb larger molecular fragments, with relatively high probabilities to desorb unfragmented molecular ions. This desorption mechanism occurs due to the electronic excitation of surface molecules when using high energy ions.[42, 43] Although this new development shows great promise the use of MeV energy ions is limited to accelerator facilities and focusing of the energetic primary ion beam is

challenging. As a result, its use is limited to carefully selected biological problems.[44, 45] One of the major limitations of SIMS is its low sensitivity to larger molecules and very high ion suppression, which prevents separating and identifying small isobaric compounds. The latter limitation has been overcome with some new advances, such as a parallel tandem MS (MS/MS) system on the TRIFT II *nano*-TOF[46] and fusion with the Thermo Orbitrap.

Matrix-assisted laser desorption/ionization (MALDI) is the most commonly used MSI technique with the widest applications in different biomedical fields, due to its high sensitivity, speed, broad molecular mass range (approx. 30 000 Da on tissue sections) and spatial resolution. The use of MALDI for the imaging of biological tissue samples is often performed *in situ* with thin tissue sections (8–16 µm). Samples for analysis are often subjected to different sample preparation strategies to improve the detection of the molecular species in question.[47] In MALDI, an analyte is co-crystallized with a matrix in a molar ratio of 10^{-2}–10^{-6}. The sample is then laser irradiated with nanoseconds of UV-laser impulsions, whose energy is absorbed by the matrix molecules. Ions are produced by an excess of protons above the surface due to the fragmentation of the acidic matrix molecules.

Commonly, MALDI is used with one of two different laser types, the N2 (337 nm) or neodymium-doped yttrium aluminum garnet (Nd:YAG; 355 nm) lasers, with repetition rates of 200–1000 Hz and typical pulse lengths of ≤3 ns. Over time, the laser spot size was reduced from 100–150 to 20 µm[48] and then 1 µm, allowing the direct imaging of single cells and tissues at subcellular spatial resolution using a transmission geometry configuration.[49] In addition to spatial resolution, breakthroughs in acquisition speed have recently been made. For example, the rapifleX MALDI Tissuetyper™ (Bruker) enables acquisition rates up to 50 pixels/s with a 10-kHz laser and two scanning mirrors that allow the laser beam to be rapidly moved across the sample.[50] Several studies have demonstrated the potential of MALDI for imaging specific peptides and protein compounds; these include the distribution of neuropeptides,[51, 52] tumor delineation in the pituitary gland,[53] molecular phenotyping of CNS glial cells[54] and endogenous peptide markers for Usher's[55] and Parkinson's diseases.[56]

Desorption electrospray ionization (DESI) imaging is a relatively new MSI technique, emerging from the laboratory of Cooks et al. in 2004.[57] DESI combines the advantages of electrospray ionization (ESI) and other desorption ionization techniques such as SIMS and laser

desorption, without the need for matrix application, making it fast and easily automatable. Solid samples produce gaseous, multiply charged ions in the form of $[M+nH]^{n+}$ or $[M-nH]^{n-}$, a characteristic feature of the ESI method. To perform DESI imaging, the sample is placed onto a target which can be a glass slide, an ITO slide or directly *in situ*. The surface to be analyzed is mounted on a movable stage in aid of proper sample positioning. Solvent is electrosprayed under gas-assisted supersonic conditions onto the sample through a nozzle, which produce desorbed ions at ambient temperature. The most common DESI probe design allowed a lateral resolution of better than 400 μm on rat brain tissue[58] but with a use of "edge sampling" the lateral resolution was improved to 40 μm.[59] DESI has many advantages that enable its application in many different areas. First, it does not require matrix application, which allows faster sample preparation and facilitates detection of low mass species. Second, biomolecules are ionized at ambient temperature, enabling the study of tissue surfaces in a non-destructive manner.[57] Third, DESI can be combined with different mass spectrometers and mass analyzers.[57, 60] DESI has been combined with an ion-mobility TOF mass spectrometer to probe the conformations of proteins desorbed from an insulating surface[59] and also linked with a linear trap quadrupole (LTQ)-based mass spectrometer (**Figure 3**). DESI has been deployed for the rapid profiling of bacteria without any sample preparation,[61] the detection of explosives[62, 63] and plant tissue profiling for alkaloid distribution (first MSI experiment).[57] DESI has been used also to study brain lipids,[64, 65] natural products in algae[66] and antifungal molecules in seaweed.[67] The detection of drugs in the brain is also possible using DESI[68] with the potential to detect drugs, drug metabolites and endogenous compounds in the same experiment. Other applications in the biomedical field as well as in pharmaceutical/industrial and forensics sciences will likely be explored.[69]

Reactive DESI. An important modification was made to DESI, termed reactive DESI, in 2009.[70] Reactive DESI sprays reagent solutions, that react very quickly with the targeted molecular entity, contrary to the conventional solvent spray. In one study, betaine aldehyde was incorporated in the spray solvent to react with the alcohol group of cholesterol by nucleophilic addition forming a hemiacetal salt. Using this set-up, the spatial distribution of cholesterol was quantitatively determined in human serum and rat brain tissues, respectively.[70] Reactive DESI is very useful for studying the spatial distribution of lipids and their profiles, successfully increasing the signal-to-noise ratio of low mass lipids in the range of *m/z* 250–350 and of phosphoethanolamines in rat brain and zebrafish tissues.[71] Reactive DESI can also distinguish

healthy from injured rat spinal cord by detecting eicosanoid compounds from lipid peroxidation in the injured samples. Dinitrophenylhydrazine (DNPH) at 100 ppm has been added to the solvent for the reactive DESI experiments, and the images were obtained in negative and positive ion modes.[72] Unfortunately, quantification from these images was not possible due to the differences in ionization efficiency. As one of the newer MSI techniques, reactive DESI will benefit from further development and optimization.

Complementary approaches. As noted, all three techniques have certain limitations, which can be overcome by their complementary characteristics. It is imperative to select the method that best meets the research question posed.[73] Regardless of the selected method, sample integrity must be maintained for proper analysis. Appropriate sample preparation is thus paramount, which is reviewed in detail elsewhere.[21, 23] MSI can be complemented with *in vivo* molecular techniques such as MRI. Combined, MSI and MRI have been used to study drug delivery in a rat brain perfusion model[74] as well as the spatial distribution of alkaloids in plants and fruits.[75] MSI and MRI can be used to study the whole body[76] as well as individual organs. For example, co-registration of the data obtained from MALDI with that from MRI and immunohistochemistry (hematoxylin and eosin staining) using PAXgene fixation provided 3D information about the kidney post-infection, an approach that could be applied to other clinically relevant questions.[77, 78]

MONITORING DRUG DELIVERY AND METABOLISM IN THE BRAIN USING MSI

MSI has been applied for the study of neurodegenerative diseases and biomarker studies over the last decade, including research on the distribution of Aβ peptides that co-localize with different elements,[79, 80] neuropeptides in Parkinson's disease[56] and global changes in phospholipid distributions in the 5xFAD transgenic mouse model for Alzheimer's disease.[81] MSI offers the unique capability of simultaneously detecting the hallmark morphological changes as well as related biomarkers of neurodegeneration, making it a powerful monitoring tool for the pathogenesis and classification of these diseases. MSI also has been successfully used for imaging drug distribution in different organs, such as clozapine and its metabolites in the brain, lung and kidney by DESI,[68] the NHBA neuroprotective drug in a whole body mouse tissue section by DESI[82] and crystal-like structures in rabbit kidney by complementary DESI and SIMS.[83] Using MSI, it was possible to determine if a drug penetrated the BBB by correlating the

location of the drug with the heme of blood cells (**Figure 3**).[84] Once the drug reaches the brain, MSI can also determine the distribution of the compound and its metabolites.[85] Only a few pharmaceuticals aimed at the treatment of brain disorders have reached the market (3–5%) in the last decade due to the inability of most active compounds to cross the BBB.[1] Direct injection into the striatum, circumventing the BBB entirely, has been used to deliver monoclonal antibodies bevacizumab and palivizumab to the brain to block angiogenesis of glioblastomas,[86] but this method is not appropriate for all compounds. Many drug delivery strategies to the brain have focused on penetrating the BBB.

Penetrating the BBB. Though the BBB is a tight membrane junction restricting the entry of most entities, several strategies have enabled the passage of drugs. Small molecules of >500 Da with high lipid solubility may penetrate the BBB by passive diffusion. Therefore, drugs can be incorporated into liposome-based particles for delivery to the brain.[87] Other carriers, such as the cell-penetrating peptide TAT (Trans-Activator of Transcription) from HIV to treat Huntingtin's disease, have been used.[88] The permeability of the BBB has been increased by using sildenafil and vardenafil that inhibit phosphodiesterase 5 to improve the penetration of anti-tumor drugs into the brain.[89] Alternatively, drug delivery can take advantage of influx changes in the BBB caused by CNS-related diseases, intracranial cell implantation or *ex-vivo* methods.[90-92] Other strategies involve locally disrupting the BBB. One interesting and very promising method uses focused ultrasound to open the barrier.[93] This method was used to treat glioblastomas in rats with induced tumors: A 400-KHz focused ultrasound was used to stimulate the BBB by delivering burst-tone ultrasound energy combined with microbubbles for increased penetration of 1,3-bis(2-chloroethyl)-1-nitrosourea (BCNU) to glioblastomas.[94] This strategy successfully enabled the drug to penetrate the brain and reach the tumor area. In another approach, a hyperosmotic solution was injected in the superficial temporal artery to open the BBB for a short time. The hyperosmotic solution forms temporary gaps and spaces, allowing the drug to diffuse into the brain and into the tumor.[95] Finally, nanoparticles (NPs) and various polymers can be designed to have the right features to reach the region of interest in the brain. In the last decade, NPs are considered one of the most powerful ways to penetrate the BBB to reach the brain.

NANOPARTICLES AND DRUGS IN CELLS: EVALUATING UPTAKE AND TOXICITY BY MSI

With their nanoscale size and customizable design, NPs have vast potential to carry and deliver active compounds to target sites. Many characteristics of NPs must be considered in drug delivery, including the effects of their size, shape and charge, the nanostructure itself and its interaction with cells and tissues, including uptake, intracellular distribution and toxicity. The physiochemical properties of NPs can be used to facilitate the controlled trigger and release of the drug cargo, with special consideration for controlled trafficking towards targeted cellular compartments such as the cytosol, nucleus and mitochondria. Until now, fluorescence imaging techniques, which require labeling the materials and various organelles, were used to visualize the co-localization of NPs with organelles in cells. Fluorescence microscopy is hampered by the inability to directly image the carrier and the cargo molecules simultaneously in the cell.[87, 96-98]

MSI offers many advantages over fluorescence microscopy for the characterization of NPs. MSI can perform targeted analysis of NPs, its cargo, the metabolites and by-products. SIMS, in particular, provides superior lateral resolution (sub-micron resolution) for this type of analysis.

A great advantage of TOF-SIMS–based techniques is the capability of performing depth profiling combined with MSI to produce 3D molecular images of cells and the analytes of interest. Applied to NPs, SIMS directly visualizes co-localized regions of NPs and drugs of interest at submicron lateral resolution and nanometer depth resolution. 3D SIMS analysis showed the distribution of the anti-arrhythmia compound amiodarone and its metabolites in NR8383 cells, an immortalized cell line derived from the lung (**Figure 4a**). With the simultaneous detection of the drug and its metabolites, isotopic labels are not needed. This was shown with the detection of desethylamiodarone metabolized by cytochrome P450.[99] NPs have been previously localized in cells, demonstrated with TiO_2[100] and polymer NPs, and due to their specific molecular signature, they could be easily identified without further processing. MSI of NPs can encounter problems with overlapping cell peaks. Graham et al. increased the signal from the potential intrinsic cell peak using a background subtraction method to image micelle polymer NPs within endosomal compartments to overcome this problem.[101] The method clearly demonstrated the isolation of NP related compound peaks.

An example where SIMS and optical microscopy can provide complementary information about the localization and uptake/release processes of NPs and associated drug in HeLa cells was shown by Proetto et al. In their work they combined illumination spectroscopy (SIM) and dynamic SIMS on the Cameca NanoSIMS to probe the polymeric NP Cy-^{15}N-NP and its drug cargo ^{195}Pt (Figure 4b.). The combination of the two techniques creates an imaging platform that can monitor the composition and integrity of the NP and its cargo from the cellular internalization to the drug release processes.[98]

Quantification: how low can we go?

Micro-scale quantification. In addition to the aforementioned qualitative characteristics of NPs and their cargo in cells, quantification of drug levels in tissue (micro-scale quantification) is critical for pharmacokinetics to understand the different mechanisms underlying a drug's efficiency or toxicity. Before the development of MSI, autoradiography was the method of choice to quantify and visualize drug distributions in animals. However, autoradiography has some technical limitations as it is based on the detection of radioactivity. Moreover, many drug candidates cannot be assessed by autoradiography because it is not practical to synthetize a radiolabeled form of each candidate molecule.

To quantify NPs, additional parameters must be considered. First, the NPs, liposomes or micelles used can increase the local drug concentration gradients in the targeted areas of the brain. Because NPs must be fully biodegradable,[102, 103] detecting NPs and their degradation products may be difficult if the biodegradation is very quick. Some other techniques have been used to determine the biodistribution and quantification of NPs. NPs have been visualized using systems able to image fluorescent and bioluminescent reporters. In fact, Liu et al. used the Caliper IVIS Spectrum Imaging System (PerkinElmer, MA, USA) to perform semi-quantitative studies on the brain, evaluating an epileptic drug delivery system loaded with a near-infrared dye.[104] It is also possible to visualize and quantify NP's using the more conventional *in vivo* MRI for drugs that preferentially accumulate in brain tumor tissues rather than healthy brain tissues.[105, 106] With the new techniques available that allow for high spatial (sub-micrometer) resolution,

such as SIMS,[107] it is now possible to determine whether NPs are located close to the targeted cells or incorporated the walls of these cells. As another micro-scale quantification strategy, gold nanoparticles are easy to detect, less toxic to tissues, and amenable to synthesis and functionalization, thus are used for many biomedical applications[108] including targeted drug delivery.[109] Despite their wide application, gold nanoparticles still require much optimization. The relative quantification of gold nanoparticles can be accomplished using inductively-coupled mass spectrometry (ICP-MS), which can detect metals at low concentration. This analysis is performed by ionizing the sample with a plasma flame and analyzing the plasma to separate and quantify the ions.[110] When coupled to a laser LA-ICP-MS can be used as an imaging technique to study the NP-based therapeutic delivery into the brain with achieving subcellular 1μm spatial resolution.[111]

PET is a nuclear medicine, functional imaging method used to observe metabolic processes in the body but can also detect NPs. PET detects pairs of gamma rays emitted by a tracer injected in the cells or in the NPs, allowing quantification by tracking total radioactivity in the brain. For example, PET has been used to detect polymer NPs within the brain by using a radioligand to test different NP sizes and their biodistribution. Sirianni et al. developed a new technique for labeling NPs with an F-18-biotin derivative.[112] PET has also been used to study BBB permeability with labeled gold nanoparticles in rodents to evaluate the most efficient drug delivery system.[113] Different NPs can be studied using PET, such as boron. PET has been deployed to evaluate the best method to perform boron neutron capture therapy (BNCT),[114] which has been used to treat malignant brain tumors such as glioblastoma). This binary technique is based on the accumulation of boron-10 in tumor cells, which is then irradiated with low-energy neutrons to induce a fission reaction to produce irreparable DNA damage to cells containing boron-10; for this reason, accumulation of boron-10 must be selective for malignant tissue only.[115]

As another nuclear-based imaging technique, single-photon emission computed tomography (SPECT) delivers a gamma-emitting radioisotope into the animal or the patient or by a radio-ligand attached to the NPs. This method allows biodistribution imaging of ultra-small NPs such as gadolinium-based NPs after their intravenous injection in rats.[116] These particles absorb the photons and release photoelectrons and Auger electrons to damage the cells by the

creation of the reactive oxygen species. These NPs are used for radiation therapy to treat brain tumors. Gadolinium can also be used as a positive contrast agent in MRI.[116, 117] Compared to PET and SPECT, MRI is easier to use for monitoring drug delivery to and in the brain.

MSI can be applied to quantify levels of a compound and its metabolites in tissue. MALDI-based MSI has some limitations in performing quantitative analysis generally attributed to poor ion-signal reproducibility resulting from heterogeneous matrix crystallization, sample variation, tissue-specific ion suppression and laser energy fluctuation but most of them can be tackled with the appropriate use of an internal standard. Chumbley et al. applied an internal standard on top of liver tissue sections to quantify Rifampicin using MALDI and obtained comparable results to liquid-chromatography mass spectrometry.[118] Furthermore, quantification requires a standard calibration curve; to perform quantification, the obtained concentration for each region of interest or for the full tissue section is plotted against the calibration curve to determine the drug amount in the tissue. MSI quantification is facilitated by dedicated software programs, such as msIQuant and Quantinetix,[119, 120] which generates normalization against an internal standard upon selecting the ion of interest (**Figure 5**).

Different MSI techniques have been used for micro-scale quantification of NPs. Laser desorption/ionization LDI, similar to MALDI but without using a matrix, can determine the biodistribution of NPs at attomole levels, making this method a potential tool for clinical analyses of biopsies and microbiopsies.[121] MALDI has been used to quantify carbon-based NPs in the brain using the intrinsic carbon cluster fingerprint signal of the carbon NPs and a calibration curve established by tissue homogenates spiked with several concentrations of carbon.[122]

Nano-scale quantification, the analysis of NPs at the cellular level, is important to evaluate a drug's ability to penetrate cells. For example, effective BNCT depends on how much boron-10 accumulates in tumor cells; therefore, quantification of boron-10 enables optimization of BNCT conditions. The first experiment using MSI to study the boron distribution in single cells was performed by Smith et al. in 1996 using an imaging mode of SIMS.[123] They showed that the concentration of boron-10 was 3.5 times higher in the main tumor mass than in normal brain tissue, opening the door for nano-scale quantification. Five years later, the authors quantified the

ratio of boron in the brain to treat glioma and gliosarcoma by using a CAMECA IMS-3F ion microscope, pixel-to-pixel registration and ratio of the boron-10 and ^{12}C images assuming 85% water content.[123] A similar protocol has been used to perform subcellular quantification using SIMS on glioblastoma with a spatial resolution of 500 nm to test different treatment times. Furthermore, the subcellular distribution of boron-10 NPs within the nucleus and the cytoplasm was demonstrated.[124] SIMS has also been used to demonstrate the heterogeneity of boron distribution depending of the cell cycle, which reveals the potential of MSI to investigate cellular events at different physiological points.[125] Chandra et al. were also able to quantify the boron-10 concentration in three subcellular compartments of the nucleus, the nucleus itself, the mitochondria-rich perinuclear cytoplasm and the cytoplasm to compare the penetration efficiency of boron. They showed that boron-10 was distributed evenly throughout the cell with the exception of the perinuclear cytoplasmic region.[126] MSI allows also the study and the optimization of boron delivery agents and injection sites to evaluate the best candidates and methods based on the biodistribution of the particles in the brain, tumor tissues and the blood.[127]

Nano-scale quantification can also be performed using proton-induced X-ray emission spectroscopy (micro-PIXE), a technique used to measure the absorbed microparticles on the lorica of marine zooplankton species.[128] Tomíc et al. used micro-PIXE to study the absorption of gold particles by human dendritic cells and demonstrated that smaller gold nanoparticles effectively accumulated and had stronger inhibitory effects on the maturation and antitumor functions of dendritic cells inducing necrosis of tumor cells. They concluded that smaller gold particles have the best potential to be used in photothermal therapy and cancer diagnostics due to their ability to penetrate cells.[129, 130]

CONCLUSIONS

The current review describes the vast potential of MSI in nanomedicine. It has proven itself as an rapidly maturing technique the study of the distribution of drugs, metabolites and nanoparticles in cells and tissues. It is very important to choose an MSI technique suited to the molecules or elements at the heart of the research question posed. We have discussed the challenges posed by the BBB in developing important therapeutics to combat many diseases, and the possibility of using MSI to assist in understanding the penetration mechanisms of drugs and NPs through the BBB. We have demonstrated that the new developments in MSI during the last decades allow us

to study the composition, distribution and quantification of drugs and their metabolites in tissue, as well as the uptake, intracellular distribution and toxicity of NPs in cells.. The three techniques reviewed here—MALDI, SIMS and DESI—are complementary and allow a better understanding of the functionalities of these particles as the drug carrier as well as the cargo itself. MSI allows the detection of both the drugs, their nanoparticle carriers and their (bio-) degradation products. In summary, MSI has proven its role to unravel mechanisms during the optimization of nanoparticle therapeutic designs, while monitoring pathogenesis of different neurodegenerative diseases and therefore, opening doors to great breakthroughs in neurosciences.

Acknowledgments

The work was performed in the M4I research program that was financially supported by the Dutch Province of Limburg as part of the "LINK" program. F.P.Y.B. acknowledges financial support from the European Union's Horizon 2020 research and innovation programme under Marie Sklodowska-Curie Program, TargetCare (ITN-2014-ETN 642414). N.O.P acknowledges financial support from FP7 European Union Marie Sklodowska-Curie IAPP Program, BrainPath (PIAPP-GA-2013-612360).

REFERENCES

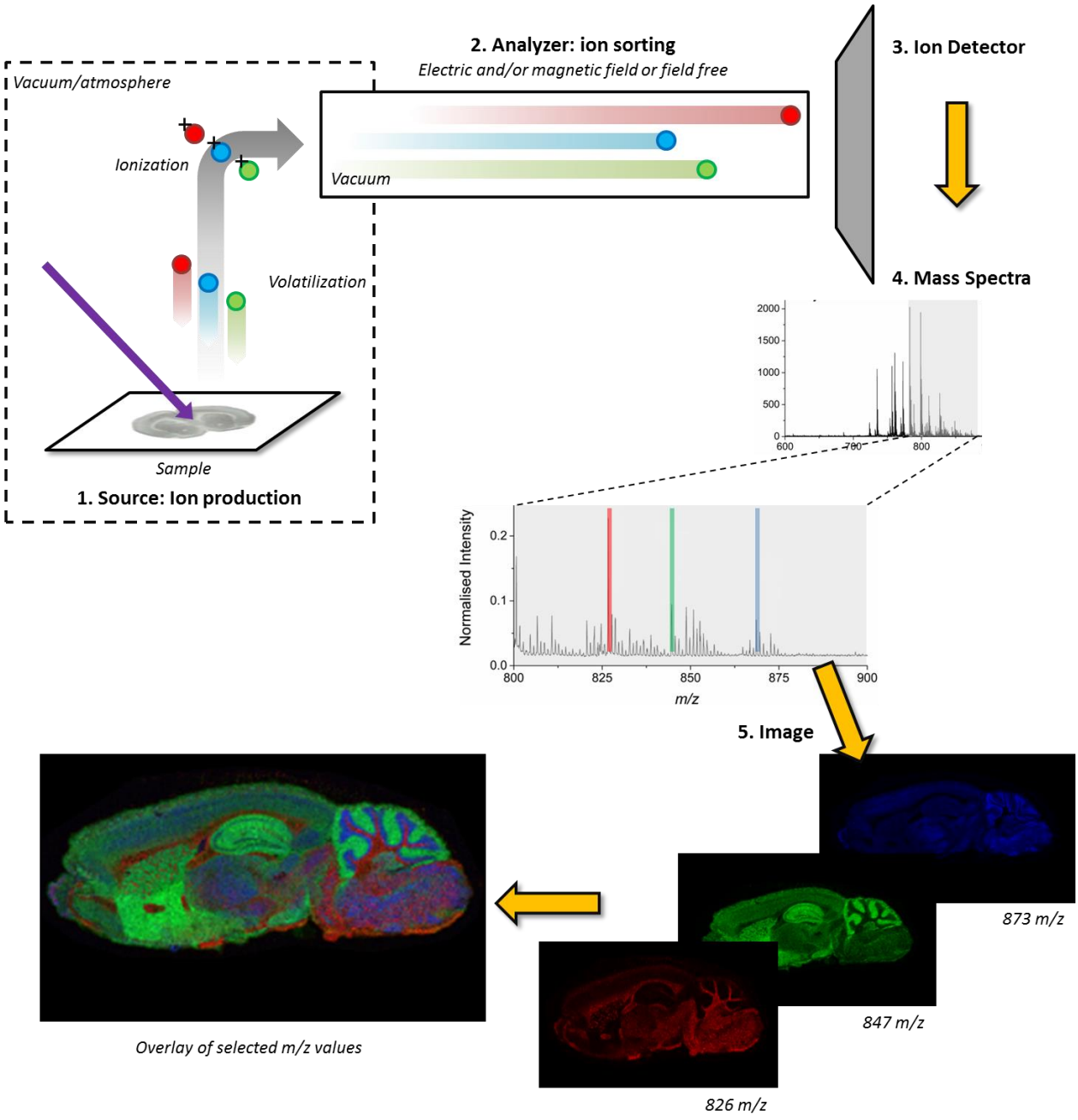

Figure 1. Mass Spectrometry Imaging workflow. 1: Production of the charged ions by the ion source from the biological tissue section mounted on a slide. The ions are charged, positively or negatively, which allow them to penetrate into the analyzer. 2: The ions penetrate the analyzer and are separated by their mass-to-charge ratio under vacuum condition by an electric/magnetic field. 3: The ions reach the detector; the lighter ions reach the detector first followed by the heavier ones. 4: Mass spectra are obtained with the different molecules corresponding to the peaks present in the spectra. Each molecule can be selected to visualize its distribution in the tissue.

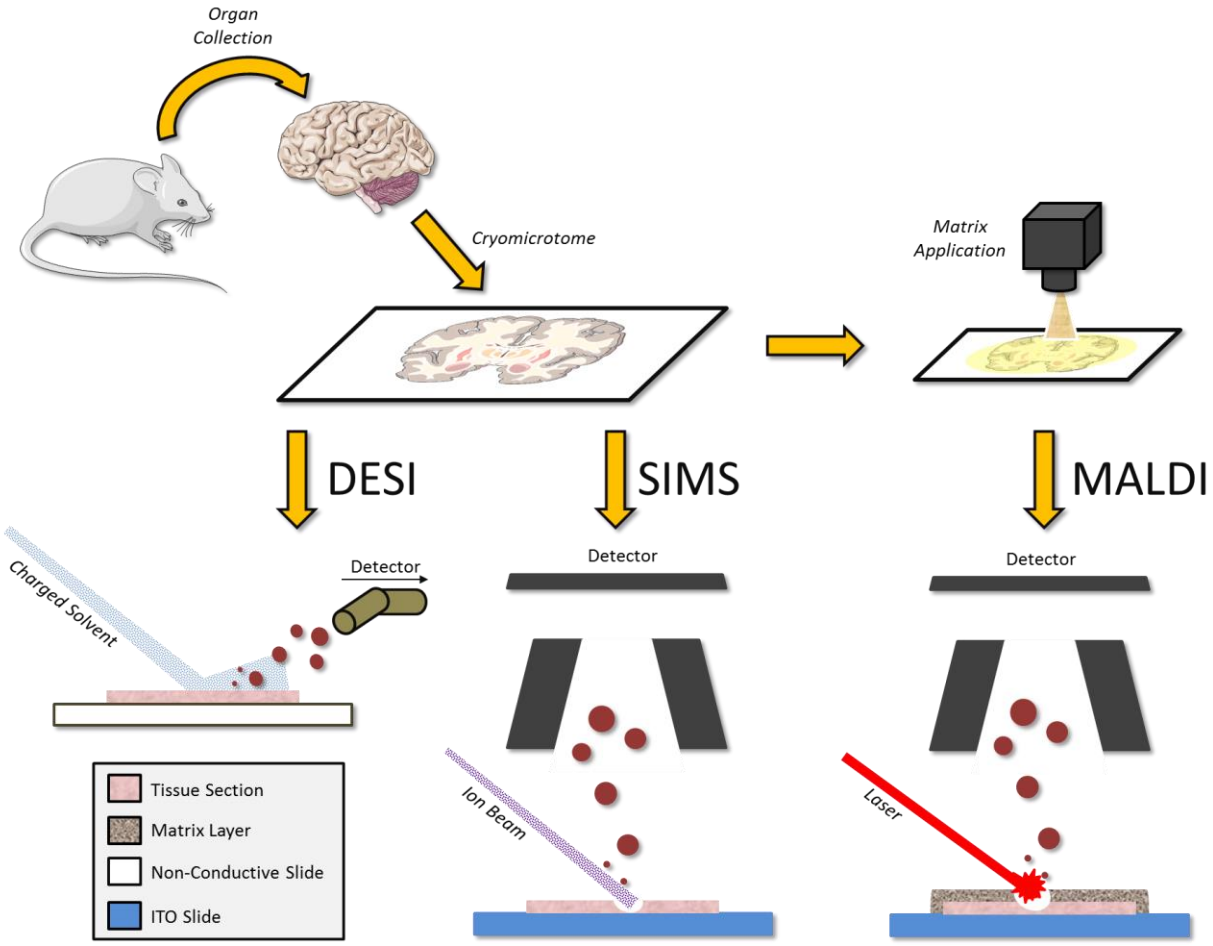

Figure 2. Overview of DESI, SIMS and MALDI MSI workflow. The organ is harvested from the animal or patient and snap-frozen or embedded in gelatin. Fresh frozen or embedded tissue is cut and mounted on a slide to perform SIMS or DESI. For MALDI, the tissue section has to be mounted on a conductive slide and a matrix has to be sprayed on top the tissue. In SIMS, an ion beam bombards the surface of the tissue, generating secondary ions for detection. In DESI, a charged solvent extracts the ions from the tissue for detection. In MALDI, a laser beam with the help of the matrix generates ions for detection.

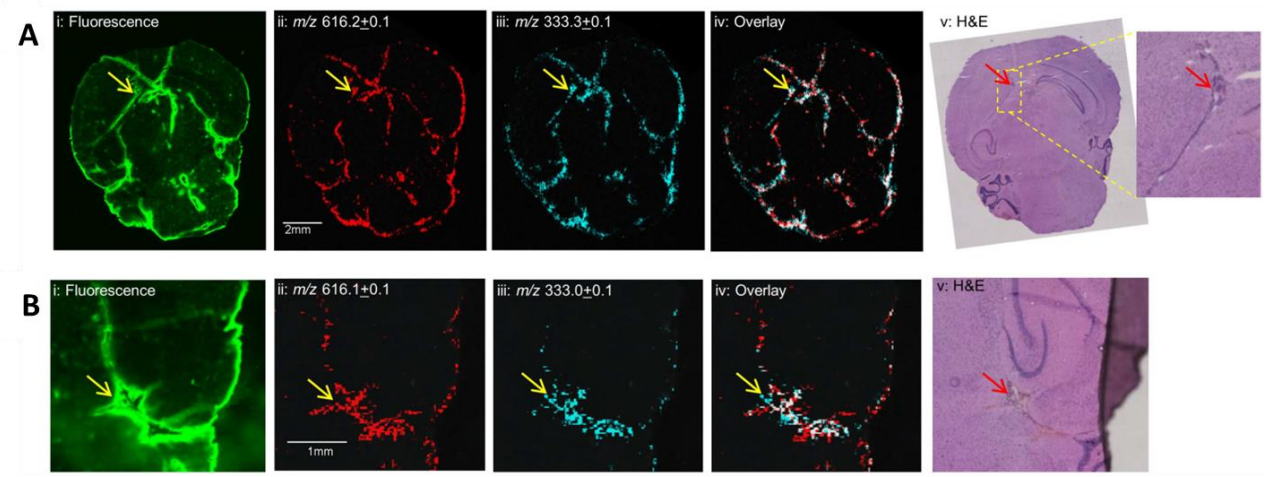

Figure 3. Comparison of heme and fluorescein images from MALDI-TOF MSI at 50-mm (A) and 25-mm (B) resolution with fluorescence image in the same mouse brain section (10-mm thickness) with pre-injected fluorescein. i: fluorescence image of blood vessels from fluorescein (excitation at 490 nm, emission at 520 nm); ii: heme image (red, *m/z* 616.2 ± 0.1 (top) and 616.1 ± 0.1 (bottom)) from MALDI MSI; iii: fluorescein image (blue, *m/z* 333.3 ± 0.1 (top) and *m/z* 333.0 ± 0.1 (bottom)) from MALDI MSI; iv: overlay of heme (red) and fluorescein (blue) from MALDI MSI. In i–iv, yellow arrows indicate the lateral ventricle delineated by fluorescein with the absence of heme. v: H&E staining of a sister section from (A) with the expanded view showing the lateral ventricle; The red arrows indicate the region of blood.

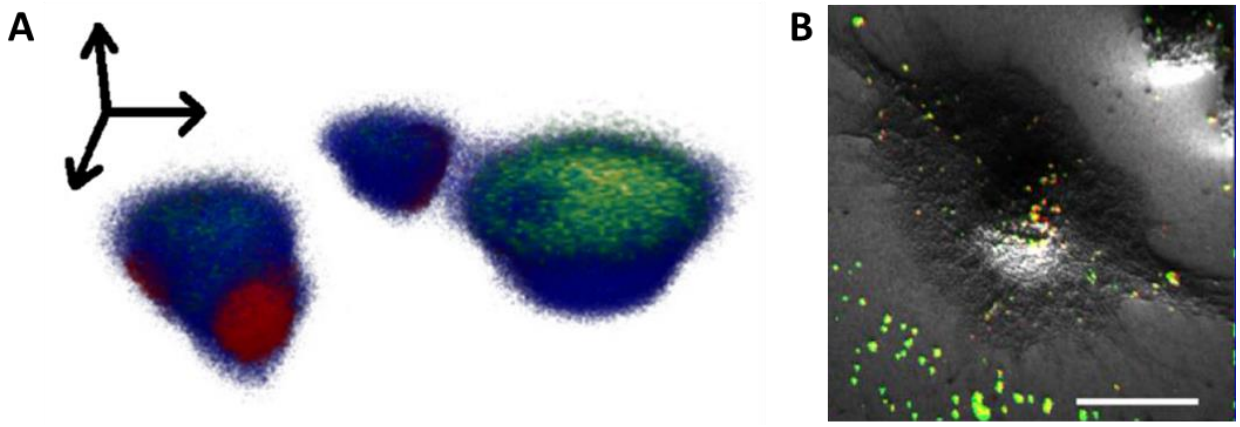

Figure 4. Imaging nanoparticles. A. 3D rendering of macrophages dosed with amiodarone. The internal distribution of amiodarone (*m/z* 640.0, green) is visible after the surface of the cells was sputtered away (1.85×10^{14} Ar_{2000}/cm^2, slices 5–40). The blue and red pixels represent the distribution of the lipid markers at *m/z* 184.1 and the nuclear-markers at *m/z* 81.0, respectively. Adapted with permission from Passarelli et al. Single-Cell Analysis: Visualizing Pharmaceutical and Metabolite Uptake in Cells with Label-Free 3D Mass spectrometry Imaging. Anal Chem. 2015 Jul 7;87(13):6696-702. doi: 10.1021/acs.analchem.5b00842. Epub 2015 Jun 23. Copyright 2015 American Chemical Society. B: Composite NanoSIMS image of a HeLa cell incubated with 15 µM Cy-^{15}N-NP where ^{195}Pt (red) and ^{15}N enrichment (green) and overlaid on the secondary ion image. Yellow regions indicate colocalization of signals. The scale bar represents 10 µm. Adapted with permission from Proetto et al. Cellular Delivery of nanoparticles revealed with Combined Optical and Isotopic Nanoscopy. *ACS Nano*, 2016, 10 (4), pp 4046–4054. Copyright 2016 American Chemical Society.

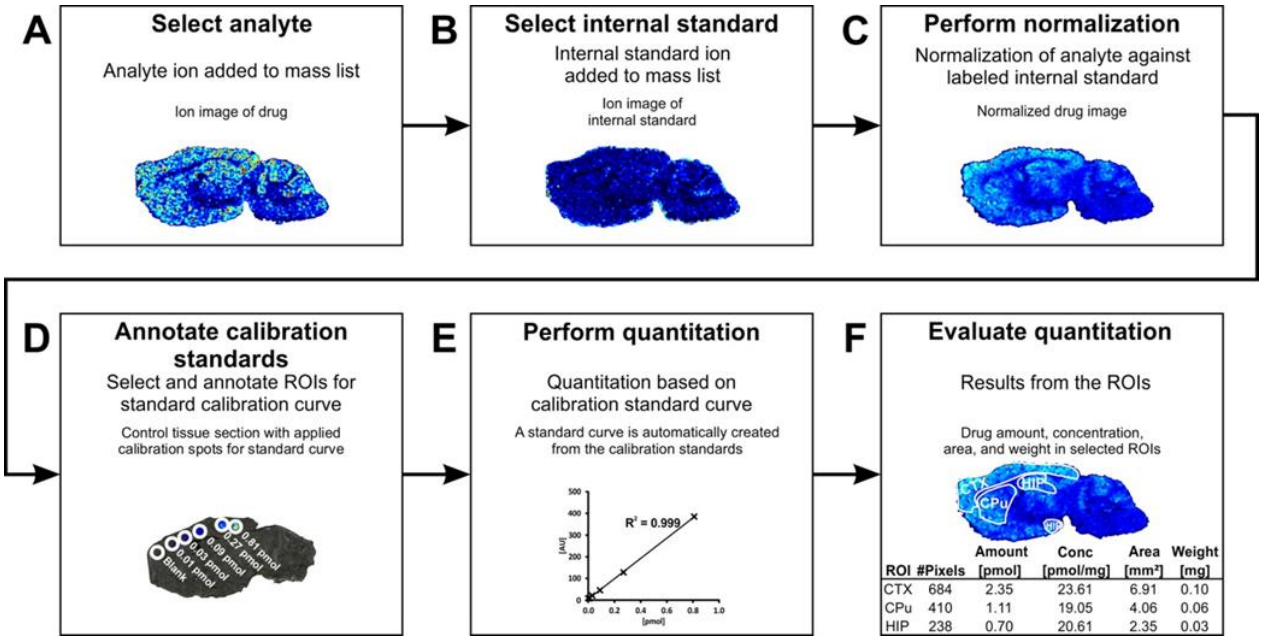

Figure 5. Quantification protocol using msIQuant. The workflow for utilizing the software is exemplified by the analysis of a brain tissue section from an animal that had been treated with a drug. (A) Ion image of the drug from a sagittal mouse brain tissue section and (B) ion image of an isotope-labeled internal standard that was applied to the tissue section before matrix application. (C) The drug's ion intensity is then normalized in each pixel using the data for the internal standard. (D) A calibration standard curve is created by applying known quantities of the drug to separate regions of a control mouse brain tissue section and then selecting and annotating the corresponding regions of interest (ROIs). The internal standard is also applied to the tissue section before matrix application and the ion intensity is normalized in each pixel using the internal standard. (E) A calibration standard curve is automatically created using the data for the normalized calibration standards. (F) Three different brain regions, cortex (CTX), hippocampus (HIP), and caudate-putamen (CPu), are selected as ROIs, and the drug concentrations (pmol/mg) and amounts (pmol) in each are calculated using the evaluation function of msIQuant. Reprinted with permission from Kallback et al. msIquant – Quantitation Software for Mass Spectrometry Imaging enabling Fast Access, Visualization, and Analysis of Large Data Set. Anal Chem. 2016 Apr 19;88(8):4346-53. doi: 10.1021/acs.analchem.5b04603. Epub 2016 Apr 5. Copyright 2016 American Chemical Society.

1 W. M. Pardridge, *Pharm Res* **2007**, *24*, 1733-44 10.1007/s11095-007-9324-2.

2 M. Karas, F. Hillenkamp, *Anal Chem* **1988**, *60*, 2299-301.

3 F. Hillenkamp, M. Karas, R. C. Beavis, B. T. Chait, *Anal Chem* **1991**, *63*, 1193A-1203A.

4 J. B. Fenn, M. Mann, C. K. Meng, S. F. Wong, C. M. Whitehouse, *Science* **1989**, *246*, 64-71.

5 E. Schoenbauer, P. Szomolanyi, T. Shiomi, V. Juras, S. Zbyn, L. Zak, M. Weber, S. Trattnig, *Journal of Biomechanics* **2015**, *48*, 3349-3355 10.1016/j.jbiomech.2015.06.016.

6 Y. Hirata, Y. Inaba, N. Kobayashi, H. Ike, Y. Yukizawa, H. Fujimaki, T. Tezuka, U. Tateishi, T. Inoue, T. Saito, *Journal of Orthopaedic Research* **2015**, *33*, 78-83 10.1002/jor.22717.

7 D. Isik, C. Isik, N. Apaydin, Y. Ustu, M. Ugurlu, M. Bozkurt, *Clinical Anatomy* **2015**, *28*, 672-677 10.1002/ca.22550.

8 Z. Fan, L. M. Sun, Y. J. Huang, Y. Z. Wang, M. J. Zhang, *Nature Nanotechnology* **2016**, *11*, 388-+ 10.1038/Nnano.2015.312.
9 M. J. Sun, B. Sun, Y. Liu, Q. D. Shen, S. J. Jiang, *Scientific Reports* **2016**, *6*, Artn 22368

10.1038/Srep22368.
10 J. Hanrieder, P. Malmberg, A. G. Ewing, *Biochimica Et Biophysica Acta-Proteins and Proteomics* **2015**, *1854*, 718-731 10.1016/j.bbapap.2014.12.026.
11 M. Lalowski, F. Magni, V. Mainini, E. Monogioudi, A. Gotsopoulos, R. Soliymani, C. Chinello, M. Baumann, *Nephrology Dialysis Transplantation* **2013**, *28*, 1648-1656 10.1093/ndt/gft008.
12 H. E. Bowrey, D. M. Anderson, P. Pallitto, D. B. Gutierrez, J. Fan, R. K. Crouch, K. L. Schey, Z. Ablonczy, *Proteomics Clinical Applications* **2016**, *10*, 391-402 10.1002/prca.201500103.
13 A. Nilsson, R. J. A. Goodwin, M. Shariatgorji, T. Vallianatou, P. J. H. Webborn, P. E. Andren, *Analytical Chemistry* **2015**, *87*, 1437-1455 10.1021/ac504734s.
14 J. Pol, M. Strohalm, V. Havlicek, M. Volny, *Histochemistry and Cell Biology* **2010**, *134*, 423-443 10.1007/s00418-010-0753-3.
15 P. Neubert, A. Walch, *Expert Review of Proteomics* **2013**, *10*, 259-273 10.1586/Epr.13.19.
16 M. Aichler, A. Walch, *Laboratory Investigation* **2015**, *95*, 422-431 10.1038/labinvest.2014.156.
17 C. Schone, H. Hofler, A. Walch, *Clinical Biochemistry* **2013**, *46*, 539-545 10.1016/j.clinbiochem.2013.01.018.
18 E. R. A. van Hove, T. R. Blackwell, I. Klinkert, G. B. Eijkel, R. M. A. Heeren, K. Glunde, *Cancer Research* **2010**, *70*, 9012-9021 10.1158/0008-5472.CAN-10-0360.
19 B. Cillero-Pastor, G. B. Eijkel, A. Kiss, F. J. Blanco, R. M. Heeren, *Arthritis Rheum* **2013**, *65*, 710-20 10.1002/art.37799.
20 M. Shariatgorji, P. Svenningsson, P. E. Andren, *Neuropsychopharmacology* **2014**, *39*, 34-49 10.1038/npp.2013.215.
21 K. Chughtai, R. M. A. Heeren, *Chemical Reviews* **2010**, *110*, 3237-3277 10.1021/cr100012c.
22 J. L. Norris, R. M. Caprioli, *Chemical Reviews* **2013**, *113*, 2309-2342 10.1021/cr3004295.
23 P. Chaurand, *J Proteomics* **2012**, *75*, 4883-92 10.1016/j.jprot.2012.04.005.
24 R. D. Macfarlane, D. F. Torgerson, *Science* **1976**, *191*, 920-5.
25 B. Sundqvist, P. Roepstorff, J. Fohlman, A. Hedin, P. Hakansson, I. Kamensky, M. Lindberg, M. Salehpour, G. Sawe, *Science* **1984**, *226*, 696-8.
26 G. Bolbach, A. Viari, R. Galera, A. Brunot, J. C. Blais, *International Journal of Mass Spectrometry and Ion Processes* **1992**, *112*, 93-100 Doi 10.1016/0168-1176(92)87034-C.
27 L. Van Vaeck, A. Adriaens, R. Gijbels, *Mass Spectrometry Reviews* **1999**, *18*, 1-47.
28 J. S. Fletcher, S. Rabbani, A. Henderson, P. Blenkinsopp, S. P. Thompson, N. P. Lockyer, J. C. Vickerman, *Analytical Chemistry* **2008**, *80*, 9058-9064 10.1021/ac8015278.
29 M. K. Passarelli, A. G. Ewing, N. Winograd, *Analytical Chemistry* **2013**, *85*, 2231-2238 10.1021/ac303038j.
30 A. M. Piwowar, S. Keskin, M. O. Delgado, K. Shen, J. J. Hue, I. Lanekoff, A. G. Ewing, N. Winograd, *Surface and Interface Analysis* **2013**, *45*, 302-304 10.1002/sia.4882.
31 T. B. Angerer, M. D. Pour, P. Malmberg, J. S. Fletcher, *Analytical Chemistry* **2015**, *87*, 4305-4313 10.1021/ac504774y.
32 H. Nygren, P. Malmberg, *Proteomics* **2010**, *10*, 1694-1698 10.1002/pmic.200900782.
33 K. L. Busch, B. H. Hsu, Y. X. Xie, R. G. Cooks, *Analytical Chemistry* **1983**, *55*, 1157-1160 10.1021/ac00258a040.
34 A. F. M. Altelaar, J. van Minnen, C. R. Jimenez, R. M. A. Heeren, S. R. Piersma, *Analytical Chemistry* **2005**, *77*, 735-741 10.1021/ac048329g.

35 L. Adriaensen, F. Vangaever, R. Gijbels, *Analytical Chemistry* **2004**, *76*, 6777-6785 10.1021/ac049108d.
36 A. Delcorte, N. Medard, P. Bertrand, *Analytical Chemistry* **2002**, *74*, 4955-4968 10.1021/ac020125h.
37 A. F. M. Altelaar, I. Klinkert, K. Jalink, R. P. J. de Lange, R. A. H. Adan, R. M. A. Heeren, S. R. Piersma, *Analytical Chemistry* **2006**, *78*, 734-742 10.1021/ac0513111.
38 E. R. Fuoco, G. Gillen, M. B. J. Wijesundara, W. E. Wallace, L. Hanley, *Journal of Physical Chemistry B* **2001**, *105*, 3950-3956 10.1021/jp0033317.
39 D. E. Weibel, N. Lockyer, J. C. Vickerman, *Applied Surface Science* **2004**, *231*, 146-152 10.1016/j.apsusc.2004.03.098.
40 S. C. C. Wong, R. Hill, P. Blenkinsopp, N. P. Lockyer, D. E. Weibel, J. C. Vickerman, *Applied Surface Science* **2003**, *203*, 219-222 Pii S0169-4332(02)00629-3

Doi 10.1016/S0169-4332(02)00629-3.
41 S. Sheraz, A. Barber, J. S. Fletcher, N. P. Lockyer, J. C. Vickerman, *Analytical Chemistry* **2013**, *85*, 5654-5658 10.1021/ac4013732.
42 Y. Nakata, Y. Honda, S. Ninomiya, T. Seki, T. Aoki, J. Matsuo, *Applied Surface Science* **2008**, *255*, 1591-1594 10.1016/j.apsusc.2008.05.108.
43 B. N. Jones, J. Matsuo, Y. Nakata, H. Yamada, J. Watts, S. Hinder, V. Palitsin, R. Webb, *Surface and Interface Analysis* **2011**, *43*, 249-252 10.1002/sia.3520.
44 M. J. Bailey, B. N. Jones, S. Hinder, J. Watts, S. Bleay, R. P. Webb, *Nuclear Instruments & Methods in Physics Research Section B-Beam Interactions with Materials and Atoms* **2010**, *268*, 1929-1932 10.1016/j.nimb.2010.02.104.
45 B. Jencic, L. Jeromel, N. O. Potocnik, K. Vogel-Mikus, E. Kovacec, M. Regvar, Z. Siketic, P. Vavpetic, Z. Rupnik, K. Bucar, M. Kelemen, J. Kovac, P. Pelicon, *Nuclear Instruments & Methods in Physics Research Section B-Beam Interactions with Materials and Atoms* **2016**, *371*, 205-210 10.1016/j.nimb.2015.10.047.
46 G. L. Fisher, A. L. Bruinen, N. O. Potocnik, J. S. Hammond, S. R. Bryan, P. E. Larson, R. M. A. Heeren, *Analytical Chemistry* **2016**, *88*, 6433-6440 10.1021/acs.analchem.6b01022.
47 L. A. McDonnell, R. M. A. Heeren, *Mass Spectrometry Reviews* **2007**, *26*, 606-643 10.1002/mas.20124.
48 P. J. Todd, T. G. Schaaff, P. Chaurand, R. M. Caprioli, *Journal of Mass Spectrometry* **2001**, *36*, 355-369 Doi 10.1002/Jms.153.
49 A. Zavalin, E. M. Todd, P. D. Rawhouser, J. H. Yang, J. L. Norris, R. M. Caprioli, *Journal of Mass Spectrometry* **2012**, *47*, 1473-1481 10.1002/jms.3108.
50 N. O. Potocnik, T. Porta, M. Becker, R. M. A. Heeren, S. R. Ellis, *Rapid Communications in Mass Spectrometry* **2015**, *29*, 2195-2203 10.1002/rcm.7379.
51 A. F. M. Altelaar, I. M. Taban, L. A. McDonnell, P. D. E. M. Verhaert, R. P. J. de Lange, R. A. H. Adan, W. J. Mooi, R. M. A. Heeren, S. R. Piersma, *International Journal of Mass Spectrometry* **2007**, *260*, 203-211 10.1016/j.ijms.2006.09.028.
52 S. Guenther, A. Rompp, W. Kummer, B. Spengler, *International Journal of Mass Spectrometry* **2011**, *305*, 228-237 10.1016/j.ijms.2010.11.011.
53 D. Calligaris, D. R. Feldman, I. Norton, O. Olubiyi, A. N. Changelian, R. Machaidze, M. L. Vestal, E. R. Laws, I. F. Dunn, S. Santagata, N. Y. R. Agar, *Proceedings of the National Academy of Sciences of the United States of America* **2015**, *112*, 9978-9983 10.1073/pnas.1423101112.
54 J. Hanrieder, G. Wicher, J. Bergquist, M. Andersson, A. Fex-Svenningsen, *Analytical and Bioanalytical Chemistry* **2011**, *401*, 135-147 10.1007/s00216-011-5043-y.
55 B. Chatterji, C. Dickhut, S. Mielke, J. Kruger, I. Just, S. Glage, M. Meier, D. Wedekind, A. Pich, *Proteomics* **2014**, *14*, 1674-1687 10.1002/pmic.201300558.

56 J. Hanrieder, A. Ljungdahl, M. Andersson, *Jove-Journal of Visualized Experiments* **2012**, Artn E3445

10.3791/3445.
57 Z. Takats, J. M. Wiseman, B. Gologan, R. G. Cooks, *Science* **2004**, *306*, 471-473 DOI 10.1126/science.1104404.
58 D. R. Ifa, J. M. Wiseman, Q. Y. Song, R. G. Cooks, *International Journal of Mass Spectrometry* **2007**, *259*, 8-15 10.1016/j.ijms.2006.08.003.
59 V. Kertesz, G. J. Van Berkel, *Rapid Communications in Mass Spectrometry* **2008**, *22*, 3846-3850 10.1002/rcm.3812.
60 S. Myung, J. M. Wiseman, S. J. Valentine, Z. Takats, R. G. Cooks, D. E. Clemmer, *Journal of Physical Chemistry B* **2006**, *110*, 5045-5051 10.1021/jp052663e.
61 Y. S. Song, N. Talaty, W. A. Tao, Z. Z. Pan, R. G. Cooks, *Chemical Communications* **2007**, 61-63 10.1039/b615724f.
62 Z. Takats, I. Cotte-Rodriguez, N. Talaty, H. W. Chen, R. G. Cooks, *Chemical Communications* **2005**, 1950-1952 10.1039/b418697d.
63 I. Cotte-Rodriguez, Z. Takats, N. Talaty, H. W. Chen, R. G. Cooks, *Analytical Chemistry* **2005**, *77*, 6755-6764 10.1021/ac050995.
64 K. Skraskova, A. Khmelinskii, W. M. Abdelmoula, S. De Munter, M. Baes, L. McDonnell, J. Dijkstra, R. M. A. Heeren, *Journal of the American Society for Mass Spectrometry* **2015**, *26*, 948-957 10.1007/s13361-015-1146-6.
65 A. L. Dill, D. R. Ifa, N. E. Manicke, A. B. Costa, J. A. Ramos-Vara, D. W. Knapp, R. G. Cooks, *Analytical Chemistry* **2009**, *81*, 8758-8764 10.1021/ac901028b.
66 E. Esquenazi, P. C. Dorrestein, W. H. Gerwick, *Proceedings of the National Academy of Sciences of the United States of America* **2009**, *106*, 7269-7270 10.1073/pnas.0902840106.
67 A. L. Lane, L. Nyadong, A. S. Galhena, T. L. Shearer, E. P. Stout, R. M. Parry, M. Kwasnik, M. D. Wang, M. E. Hay, F. M. Fernandez, J. Kubanek, *Proceedings of the National Academy of Sciences of the United States of America* **2009**, *106*, 7314-7319 10.1073/pnas.0812020106.
68 J. M. Wiseman, D. R. Ifa, Y. X. Zhu, C. B. Kissinger, N. E. Manicke, P. T. Kissinger, R. G. Cooks, *Proceedings of the National Academy of Sciences of the United States of America* **2008**, *105*, 18120-18125 10.1073/pnas.0801066105.
69 R. G. Cooks, Z. Ouyang, Z. Takats, J. M. Wiseman, *Science* **2006**, *311*, 1566-1570 10.1126/science.1119426.
70 C. P. Wu, D. R. Ifa, N. E. Manicke, R. G. Cooks, *Analytical Chemistry* **2009**, *81*, 7618-7624 10.1021/ac901003u.
71 D. Lostun, C. J. Perez, P. Licence, D. A. Barrett, D. R. Ifa, *Analytical Chemistry* **2015**, *87*, 3286-3293 10.1021/ac5042445.
72 M. Girod, Y. Z. Shi, J. X. Cheng, R. G. Cooks, *Analytical Chemistry* **2011**, *83*, 207-215 10.1021/ac102264z.
73 J. C. Vickerman, *Analyst* **2011**, *136*, 2199-2217 10.1039/c1an00008j.
74 K. Tabanor, P. Lee, P. Kiptoo, I. Y. Choi, E. B. Sherry, C. S. Eagle, T. D. Williams, T. J. Siahaan, *Molecular Pharmaceutics* **2016**, *13*, 379-390 10.1021/acs.molpharmaceut.5b00607.
75 A. Srimany, C. George, H. R. Naik, D. G. Pinto, N. Chandrakumar, T. Pradeep, *Phytochemistry* **2016**, *125*, 35-42 10.1016/j.phytochem.2016.02.002.
76 A. S. Attia, K. A. Schroeder, E. H. Seeley, K. J. Wilson, N. D. Hammer, D. C. Colvin, M. L. Manier, J. J. Nicklay, K. L. Rose, J. C. Gore, R. M. Caprioli, E. P. Skaar, *Cell Host & Microbe* **2012**, *11*, 664-673 10.1016/j.chom.2012.04.018.

77 J. Oetjen, M. Aichler, D. Trede, J. Strehlow, J. Berger, S. Heldmann, M. Becker, M. Gottschalk, J. H. Kobarg, S. Wirtz, S. Schiffler, H. Thiele, A. Walch, P. Maass, T. Alexandrov, *Journal of Proteomics* **2013**, *90*, 52-60 10.1016/j.jprot.2013.03.013.
78 L. Jiang, T. R. Greenwood, D. Artemov, V. Raman, P. T. Winnard, R. M. A. Heeren, Z. M. Bhujwalla, K. Glunde, *Neoplasia* **2012**, *14*, 732-741 10.1593/neo.12858.
79 N. Braidy, A. Poljak, C. Marjo, H. Rutlidge, A. Rich, T. Jayasena, N. C. Inestrosa, P. Sachdev, *Frontiers in Aging Neuroscience* **2014**, *6*, Artn 138

10.3389/Fnagi.2014.00138.
80 L. Carlred, W. Michno, I. Kaya, P. Sjovall, S. Syvanen, J. Hanrieder, *Journal of Neurochemistry* **2016**, *138*, 469-478 10.1111/jnc.13645.
81 J. H. Hong, J. W. Kang, D. K. Kim, S. H. Baik, K. H. Kim, S. R. Shanta, J. H. Jung, I. Mook-Jung, K. P. Kim, *Journal of Lipid Research* **2016**, *57*, 36-45 10.1194/jlr.M057869.
82 J. L. He, Z. G. Luo, L. Huang, J. M. He, Y. Chen, X. F. Rong, S. B. Jia, F. Tang, X. H. Wang, R. P. Zhang, J. J. Zhang, J. G. Shi, Z. Abliz, *Analytical Chemistry* **2015**, *87*, 5372-5379 10.1021/acs.analchem.5b00680.
83 A. L. Bruinen, C. van Oevelen, G. B. Eijkel, M. Van Heerden, F. Cuyckens, R. M. A. Heeren, *Journal of the American Society for Mass Spectrometry* **2016**, *27*, 117-123 10.1007/s13361-015-1254-3.
84 X. H. Liu, J. L. Ide, I. Norton, M. A. Marchionni, M. C. Ebling, L. Y. Wang, E. Davis, C. M. Sauvageot, S. Kesari, K. A. Kellersberger, M. L. Easterling, S. Santagata, D. D. Stuart, J. Alberta, J. N. Agar, C. D. Stiles, N. Y. R. Agar, *Scientific Reports* **2013**, *3*, Artn 2859

10.1038/Srep02859.
85 S. Okutan, H. S. Hansen, C. Janfelt, *Proteomics* **2016**, *16*, 1634-1641 10.1002/pmic.201500422.
86 R. Ait-Belkacem, C. Berenguer, C. Villard, L. Ouafik, D. Figarella-Branger, A. Beck, O. Chinot, D. Lafitte, *MAbs* **2014**, *6*, 1385-93 10.4161/mabs.34405.
87 M. Masserini, *ISRN Biochem* **2013**, *2013*, 238428 10.1155/2013/238428.
88 Y. Arribat, Y. Talmat-Amar, A. Paucard, P. Lesport, N. Bonneaud, C. Bauer, N. Bec, M. L. Parmentier, L. Benigno, C. Larroque, P. Maurel, F. Maschat, *Acta Neuropathologica Communications* **2014**, *2*, ARTN 86

10.1186/s40478-014-0086-x.
89 H. Hu, L. Jiang, H. Pu, Y. Chen, X. J. Liu, *Physical Review Letters* **2013**, *110*, Artn 020401

10.1103/Physrevlett.110.020401.
90 B. Obermeier, R. Daneman, R. M. Ransohoff, *Nature Medicine* **2013**, *19*, 1584-1596 10.1038/nm.3407.
91 B. V. Zlokovic, *Neuron* **2008**, *57*, 178-201 10.1016/j.neuron.2008.01.003.
92 H. J. van de Haar, S. Burgmans, J. F. A. Jansen, M. J. P. van Osch, M. A. van Buchem, M. Muller, P. A. M. Hofman, F. R. J. Verhey, W. H. Backes, *Radiology* **2016**, *281*, 527-535 10.1148/radiol.2016152244.
93 K. F. Timbie, B. P. Mead, R. J. Price, *Journal of Controlled Release* **2015**, *219*, 61-75 10.1016/j.jconrel.2015.08.059.
94 H. L. Liu, M. Y. Hua, P. Y. Chen, P. C. Chu, C. H. Pan, H. W. Yang, C. Y. Huang, J. J. Wang, T. C. Yen, K. C. Wei, *Radiology* **2010**, *255*, 415-425 10.1148/radiol.10090699.
95 S. Sato, T. Kawase, S. Harada, H. Takayama, S. Suga, *Acta Neurochirurgica* **1998**, *140*, 1135-+ DOI 10.1007/s007010050227.
96 Y. Cheng, R. A. Morshed, B. Auffinger, A. L. Tobias, M. S. Lesniak, *Advanced Drug Delivery Reviews* **2014**, *66*, 42-57 10.1016/j.addr.2013.09.006.

97 I. P. Kaur, R. Bhandari, S. Bhandari, V. Kakkar, *Journal of Controlled Release* **2008**, *127*, 97-109 10.1016/j.jconrel.2007.12.018.
98 M. T. Proetto, C. R. Anderton, D. H. Hu, C. J. Szymanski, Z. H. Zhu, J. P. Patterson, J. K. Kammeyer, L. G. Nilewski, A. M. Rush, N. C. Bell, J. E. Evans, G. Orr, S. B. Howell, N. C. Gianneschi, *Acs Nano* **2016**, *10*, 4046-4054 10.1021/acsnano.5b06477.
99 M. K. Passarelli, C. F. Newman, P. S. Marshall, A. West, I. S. Gilmore, J. Bunch, M. R. Alexander, C. T. Dollery, *Analytical Chemistry* **2015**, *87*, 6696-6702 10.1021/acs.analchem.5b00842.
100 J. N. Audinot, A. Georgantzopoulou, J. P. Piret, A. C. Gutleb, D. Dowsett, H. N. Migeon, L. Hoffmann, *Surface and Interface Analysis* **2013**, *45*, 230-233 10.1002/sia.5099.
101 D. J. Graham, J. T. Wilson, J. J. Lai, P. S. Stayton, D. G. Castner, *Biointerphases* **2016**, *11*, Artn 02a304

10.1116/1.4934795.
102 A. Mahapatro, D. K. Singh, *Journal of Nanobiotechnology* **2011**, *9*, Artn 55

10.1186/1477-3155-9-55.
103 T. J. Spitzenberger, D. Heilman, C. Diekmann, E. V. Batrakova, A. V. Kabanov, H. E. Gendelman, W. F. Elmquist, Y. Persidsky, *Journal of Cerebral Blood Flow and Metabolism* **2007**, *27*, 1033-1042 10.1038/sj.jcbfm.9600414.
104 J. S. Liu, Y. J. He, J. Zhang, J. J. Li, X. R. Yu, Z. L. Cao, F. M. Meng, Y. W. Zhao, X. Y. Wu, T. Shen, Z. Hong, *Biomaterials* **2016**, *74*, 64-76 10.1016/j.biomaterials.2015.09.041.
105 X. R. Yu, J. H. Wang, J. S. Liu, S. Shen, Z. L. Cao, J. W. Pan, S. Y. Zhou, Z. Q. Pang, D. Y. Geng, J. Zhang, *Biomaterials* **2016**, *76*, 173-186 10.1016/j.biomaterials.2015.10.050.
106 M. I. Koukourakis, S. Koukouraki, I. Fezoulidis, N. Kelekis, G. Kyrias, S. Archimandritis, N. Karkavitsas, *British Journal of Cancer* **2000**, *83*, 1281-1286 DOI 10.1054/bjoc.2000.1459.
107 M. Korsgen, A. Pelster, K. Dreisewerd, H. F. Arlinghaus, *Journal of the American Society for Mass Spectrometry* **2016**, *27*, 277-284 10.1007/s13361-015-1275-y.
108 P. M. Tiwari, K. Vig, V. A. Dennis, S. R. Singh, *Nanomaterials* **2011**, *1*, 31-63 10.3390/nano1010031.
109 H. Daraee, A. Eatemadi, E. Abbasi, S. F. Aval, M. Kouhi, A. Akbarzadeh, *Artificial Cells Nanomedicine and Biotechnology* **2016**, *44*, 410-422 10.3109/21691401.2014.955107.
110 F. Laborda, E. Bolea, J. Jimenez-Lamana, *Analytical Chemistry* **2014**, *86*, 2270-2278 10.1021/ac402980q.
111 H. A. O. Wang, D. Grolimund, C. Giesen, C. N. Borca, J. R. H. Shaw-Stewart, B. Bodenmiller, D. Gunther, *Analytical Chemistry* **2013**, *85*, 10107-10116 10.1021/ac400996x.
112 R. W. Sirianni, M. Q. Zheng, T. R. Patel, T. Shafbauer, J. Zhou, W. M. Saltzman, R. E. Carson, Y. Huang, *Bioconjug Chem* **2014**, *25*, 2157-65 10.1021/bc500315j.
113 J. Frigell, I. Garcia, V. Gomez-Vallejo, J. Llop, S. Penades, *Journal of the American Chemical Society* **2014**, *136*, 449-457 10.1021/ja411096m.
114 Y. Iguchi, H. Michiue, M. Kitamatsu, Y. Hayashi, F. Takenaka, T. Nishiki, H. Matsui, *Biomaterials* **2015**, *56*, 10-17 10.1016/j.biomaterials.2015.03.061.
115 T. Yamamoto, K. Nakai, A. Matsumura, *Cancer Letters* **2008**, *262*, 143-152 10.1016/j.canlet.2008.01.021.
116 I. Miladi, G. Le Duc, D. Kryza, A. Berniard, P. Mowat, S. Roux, J. Taleb, P. Bonazza, P. Perriat, F. Lux, O. Tillement, C. Billotey, M. Janier, *Journal of Biomaterials Applications* **2013**, *28*, 385-394 10.1177/0885328212454315.

117 G. Strohbehn, D. Coman, L. Han, R. R. T. Ragheb, T. M. Fahmy, A. J. Huttner, F. Hyder, J. M. Piepmeier, W. M. Saltzman, J. B. Zhou, *Journal of Neuro-Oncology* **2015**, *121*, 441-449 10.1007/s11060-014-1658-0.
118 C. W. Chumbley, M. L. Reyzer, J. L. Allen, G. A. Marriner, L. E. Via, C. E. Barry, R. M. Caprioli, *Analytical Chemistry* **2016**, *88*, 2392-2398 10.1021/acs.analchem.5b04409.
119 P. Kallback, A. Nilsson, M. Shariatgorji, P. E. Andren, *Analytical Chemistry* **2016**, *88*, 4346-4353 10.1021/acs.analchem.5b04603.
120 Z. C. Zhang, J. Kuang, L. J. Li, *Analyst* **2013**, *138*, 6600-6606 10.1039/c3an01225e.
121 B. Yan, S. T. Kim, C. S. Kim, K. Saha, D. F. Moyano, Y. Q. Xing, Y. Jiang, A. L. Roberts, F. S. Alfonso, V. M. Rotello, R. W. Vachet, *Journal of the American Chemical Society* **2013**, *135*, 12564-12567 10.1021/ja406553f.
122 S. M. Chen, C. Q. Xiong, H. H. Liu, Q. Q. Wan, J. Hou, Q. He, A. Badu-Tawiah, Z. X. Nie, *Nature Nanotechnology* **2015**, *10*, 176-182 10.1038/Nnano.2014.282.
123 D. R. Smith, S. Chandra, J. A. Coderre, G. H. Morrison, *Cancer Research* **1996**, *56*, 4302-4306.
124 S. Chandra, D. R. Lorey, D. R. Smith, *Radiation Research* **2002**, *157*, 700-710 Doi 10.1667/0033-7587(2002)157[0700:Qssims]2.0.Co;2.
125 S. Chandra, W. Tjarks, D. R. Lorey, R. F. Barth, *Journal of Microscopy-Oxford* **2008**, *229*, 92-103 DOI 10.1111/j.1365-2818.2007.01869.x.
126 S. Chandra, R. F. Barth, S. A. Haider, W. L. Yang, T. Y. Huo, A. L. Shaikh, G. W. Kabalka, *Plos One* **2013**, *8*, ARTN e75377

10.1371/journal.pone.0075377.
127 R. F. Barth, G. W. Kabalka, W. L. Yang, T. Y. Huo, R. J. Nakkula, A. L. Shaikh, S. A. Haider, S. Chandra, *Applied Radiation and Isotopes* **2014**, *88*, 38-42 10.1016/j.apradiso.2013.11.133.
128 N. Ogrinc, P. Pelicon, P. Vavpetic, M. Kelemen, N. Grlj, L. Jeromel, S. Tomic, M. Colic, A. Beran, *Nuclear Instruments & Methods in Physics Research Section B-Beam Interactions with Materials and Atoms* **2013**, *306*, 121-124 10.1016/j.nimb.2012.12.060.
129 S. Tomic, J. Dokic, S. Vasilijic, N. Ogrinc, R. Rudolf, P. Pelicon, D. Vucevic, P. Milosavljevic, S. Jankovic, I. Anzel, J. Rajkovic, M. S. Rupnik, B. Friedrich, M. Colic, *Plos One* **2014**, *9*, ARTN e96584

10.1371/journal.pone.0096584.
130 Y. P. Kim, H. K. Shon, S. K. Shin, T. G. Lee, *Mass Spectrometry Reviews* **2015**, *34*, 237-247 10.1002/mas.21437.